Inorganic Chemistry
Article

Inorg. Chem. **2010**, *49*, 11439–11448 **11439**
DOI: 10.1021/ic1015109

Thermodynamic, Electrochemical, High-Pressure Kinetic, and Mechanistic Studies of the Formation of Oxo Fe^{IV}−TAML Species in Water

Delia-Laura Popescu,[†] Melanie Vrabel,[†] Ariane Brausam,[‡] Peter Madsen,[†] Gabor Lente,[§] Istvan Fabian,[§] Alexander D. Ryabov,*[,†] Rudi van Eldik,*[,‡] and Terrence J. Collins*[,†]

[†]*Department of Chemistry, Carnegie Mellon University, 4400 Fifth Avenue, Pittsburgh, Pennsylvania 15213, United States* , [‡]*Inorganic Chemistry, Department of Chemistry and Pharmacy, University of Erlangen-Nürnberg, Egerlandstrasse 1, 91058 Erlangen, Germany, and* [§]*Department of Inorganic and Analytical Chemistry, University of Debrecen, Debrecen, Hungary*

Received July 28, 2010

Stopped-flow kinetic studies of the oxidation of Fe^{III}−TAML catalysts, $[Fe\{1,2\text{-}X_2C_6H_2\text{-}4,5\text{-}(NCOCMe_2NCO)_2CMe_2\}(OH_2)]^-$ (**1**), by *t*-BuOOH and H_2O_2 in water affording Fe^{IV} species has helped to clarify the mechanism of the interaction of **1** with primary oxidants. The data collected for substituted Fe^{III}−TAMLs at pH 6.0−13.8 and 17−45 °C has confirmed that the reaction is first order both in **1** and in peroxides. Bell-shaped pH profiles of the effective second-order rate constants k_I have maximum values in the pH range of 10.5−12.5 depending on the nature of **1** and the selected peroxide. The "acidic" part is governed by the deprotonation of the diaqua form of **1** and therefore electron-withdrawing groups move the lower pH limit of the reactivity toward neutral pH, although the rate constants k_I do not change much. The dissection of k_I into individual intrinsic rate constants k_1 ($[FeL(OH_2)_2]^- + ROOH$), k_2 ($[FeL(OH_2)OH)]^{2-} + ROOH$), k_3 ($[FeL(OH_2)_2]^- + ROO^-$), and k_4 ($[FeL(OH_2)OH)]^{2-} + ROO^-$) provides a model for understanding the bell-shaped pH-profiles. Analysis of the pressure and substituent effects on the reaction kinetics suggest that the k_2 pathway is (i) more probable than the kinetically indistinguishable k_3 pathway, and (ii) presumably mechanistically similar to the induced cleavage of the peroxide O−O bond postulated for cytochrome P450 enzymes. The redox titration of **1** by Ir^{IV} and electrochemical data suggest that under basic conditions the reduction potential for the half-reaction $[Fe^{IV}L(=O)(OH_2)]^{2-} + e^- + H_2O \rightarrow [Fe^{III}L(OH)(OH_2)]^{2-} + OH^-$ is close to 0.87 V (vs NHE).

Introduction

The family of Fe^{III}−TAML catalysts **1**[1] display impressive properties in activating peroxides, especially hydrogen peroxide, for a variety of environmentally important oxidation processes.[2−8] Fe^{III}−TAML catalysts are iron(III) complexes of quadruply deprotonated tetraamido macrocyclic ligands (Chart 1).

The catalytic cycles include the oxidation of the catalysts **1** by a primary oxidizing agent followed by the attack of the intermediates that are formed at target molecules.[9] In a number of cases, it has been possible isolate and/or spectroscopically characterize the species that are formed from the reactions of **1** and peroxides, peracids, or dioxygen under different conditions.[10−12] The current state of knowledge is summarized in Scheme 1. *m*-Chloroperbenzoic acid converts **1a** into the monomeric iron(V)-oxo species **2** in organic solvents (*n*-butyronitrile), a clean 2-electron oxidation performed by a 2-electron oxidizing agent.[10] In non-coordinating chlorinated

*To whom correspondence should be addressed. E-mail: ryabov@andrew.cmu.edu.

(1) Collins, T. J. *Acc. Chem. Res.* **2002**, *35*, 782–790.
(2) Banerjee, D.; Markley, A. L.; Yano, T.; Ghosh, A.; Berget, P. B.; Minkley, E. G., Jr.; Khetan, S. K.; Collins, T. J. *Angew. Chem., Int. Ed.* **2006**, *45*, 3974–3977.
(3) Collins, T. J.; Horwitz, C. P.; Ryabov, A. D.; Vuocolo, L. D.; Sen Gupta, S.; Ghosh, A.; Fattaleh, N. L.; Hangun, Y.; Steinhoff, B.; Noser, C. A.; Beach, E.; Prasuhn, D., Jr.; Stuthridge, T.; Wingate, K. G.; Hall, J.; Wright, L. J.; Suckling, I.; Allison, R. W. *TAML Catalytic Oxidant Activators in the Pulp and Paper Industry*; American Chemical Society: Washington, DC, 2002; pp 47−60.
(4) Chanda, A.; Khetan, S. K.; Banerjee, D.; Ghosh, A.; Collins, T. J. *J. Am. Chem. Soc.* **2006**, *128*, 12058–12059.
(5) Chanda, A.; Ryabov, A. D.; Mondal, S.; Alexandrova, L.; Ghosh, A.; Hangun-Balkir, Y.; Horwitz, C. P.; Collins, T. J. *Chem.—Eur. J.* **2006**, *12*, 9336–9345.
(6) Chahbane, N.; Popescu, D.-L.; Mitchell, D. A.; Chanda, A.; Lenoir, D.; Ryabov, A. D.; Schramm, K.-W.; Collins, T. J. *Green Chem.* **2007**, *9*, 49–57.
(7) Mitchell, D. A.; Ryabov, A. D.; Kundu, S.; Chanda, A.; Collins, T. J. *J. Coord. Chem.* **2010**, *63*, 2605–2618.
(8) Shappell, N. W.; Vrabel, M. A.; Madsen, P. J.; Harrington, G.; Billey, L. O.; Hakk, H.; Larsen, G. L.; Beach, E. S.; Horwitz, C. P.; Ro, K.; Hunt, P. G.; Collins, T. J. *Environ. Sci. Technol.* **2008**, *42*, 1296–1300.
(9) Ghosh, A.; Mitchell, D. A.; Chanda, A.; Ryabov, A. D.; Popescu, D. L.; Upham, E.; Collins, G. J.; Collins, T. J. *J. Am. Chem. Soc.* **2008**, *130*, 15116–15126.

Published on Web 11/18/2010

Chart 1. Fe^{III}–TAML Activators Used in This Work

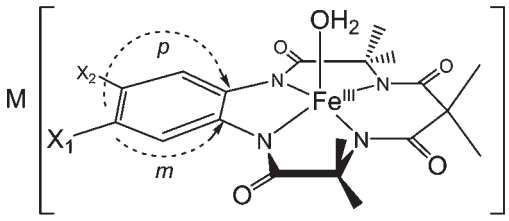

1	X_1	X_2
a	H	H
b	CH_3	CH_3
c	MeOOC	H
d	NO_2	H
e	Cl	Cl

1

Scheme 1. Oxidized Derivatives of Fe^{III}–TAMLs Generated from **1a** and Various Oxidants under Different Conditions[a]

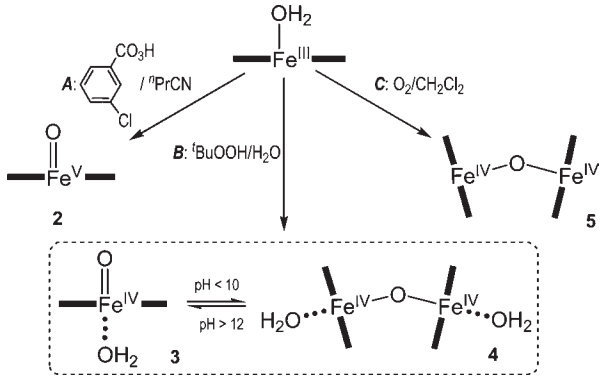

[a] Compounds **2**–**4** have been characterized spectroscopically in solution; **5** was has been extensively characterized by spectroscopy and by X-ray crystallography. Compounds **2** and **5** are five-coordinate species; weak binding of a sixth aqueous ligand cannot be excluded for **3** or **4**. Charges have been omitted for clarity. The ligation for **1a** is shown as in the solid state, but it is known to convert to six-coordinate species in water. For details on the oxidized products **2**, **3**/**4**, and **5**, see refs 10–12.

solvents, **1a** is oxidized by dioxygen into the oxo-bridged iron(IV) dimer **5**, the structure of which has been established by X-ray crystallography; **2** is proposed to be an intermediate in the formation of **5**.[11] Mössbauer and EXAFS spectroscopies support the formation of iron(IV) species formed from **1a** and ^{t}BuOOH in water—a 1-electron oxidation performed by a 2-electron oxidant with the possible intermediacy of **2**.[12] At pH > 12, the oxo iron(IV) monomer **3** is produced. At pH < 10, compound **3** dimerizes into the (μ-oxo)-bridged iron(IV) dimer **4**, which is similar to **5** produced in methylene chloride. These monomeric oxo and/or dimeric μ-oxo iron species of oxidation states IV and V could be involved as intermediates in the catalytic cycles of Fe^{III}–TAML oxidation processes.[9] Water is nature's principal solvent making it the ideal solvent for green chemistry,[1,13] and the **1** catalysts display the highest catalytic activity in this solvent.[9,14] Thus, it is desirable to understand in detail the mechanistic pathways in water that lead to the oxidized species **3** and **4** which have been previously characterized through spectroscopic techniques.[12] Here we report on the results of thermodynamic and stopped-flow (including high-pressure) kinetic studies on reactions of H_2O_2 and ^{t}BuOOH with complexes **1** (Chart 1) to afford **3** or **4** including, (i) evidence that, as with ^{t}BuOOH, H_2O_2 converts **1** into Fe^{IV} species in water; (ii) an estimation of the electrochemical properties relating **3** and **1**; (iii) an explicit mechanistic picture of the reactions of Fe^{III}–TAMLs with the primary oxidants H_2O_2 and ^{t}BuOOH. A component of the kinetic data has been preliminarily communicated.[15]

Experimental Section

General Procedures. All reagents, components of buffer solutions, and solvents were at least ACS reagent grade (Aldrich, Fisher, Acros, Fluka) and were used as received unless otherwise indicated. TAML activators **1** were synthesized at Carnegie Mellon University as indicated previously.[9,16,17] UV/vis measurements were performed using a Perkin-Elmer Lambda 900 UV/vis-NIR spectrometer equipped with a thermostatted cell holder or a Hewlett-Packard Diode Array spectrophotometer (model 8453) equipped with a thermostatted cell holder and an automatic 8-cell positioner. Electrochemical measurements were performed on a PC-interfaced potentiostat-galvanostat AUTOLAB PGSTAT 12. A three-electrode setup was used with a working glassy carbon electrode, SCE as a reference electrode, and auxiliary stainless steel electrode. Before each measurement, the working electrode was polished with a diamond paste and rinsed with water. The solution was purged with argon. The pH of solutions was measured using an Accumet AB15 or a Corning 220 pH meter, which were calibrated with standard buffer solutions at pH 4, 7, and 10. Stock solutions of the catalysts were prepared in HPLC grade H_2O or MeCN. Reagent grade H_2O_2 (30% v/v) was purchased from Fluka, and its concentration was standardized daily by measuring the absorbance at 230 nm (ε 72.8 M^{-1} cm^{-1}).[18] Reagent grade ^{t}BuOOH was purchased from Fluka as a 70% aqueous solution. Fresh stock solutions were prepared daily. All experiments were reproduced at least in triplicate. Calculations were carried out using Sigma Plot 2001 and 2006 packages (Versions 7.0 and 10.1) and Mathematica 5. UV/vis spectroscopic experiments with K_2IrCl_6 were carried out in a quartz cuvette (1 cm path length) at 25 °C and pH 11 in 0.01 M phosphate buffer using HPLC grade water. K_2IrCl_6 was stored as a 10 mM solution containing 0.01 M HCl since the compound is unstable above neutral pH over an extended period of time. Further

(10) Tiago de Oliveira, F.; Chanda, A.; Banerjee, D.; Shan, X.; Mondal, S.; Que, L., Jr.; Bominaar, E. L.; Münck, E.; Collins, T. J. *Science* **2007**, *315*, 835–838.
(11) Ghosh, A.; Tiago de Oliveria, F.; Toshihiro Yano, T.; Nishioka, T.; Beach, E. S.; Kinoshita, I.; Münck, E.; Ryabov, A. D.; Horwits, C. P.; Collins, T. J. *J. Am. Chem. Soc.* **2005**, *127*, 2505–2513.
(12) Chanda, A.; Shan, X.; Chakrabarti, M.; Ellis, W.; Popescu, D.; Tiago de Oliveria, F.; Wang, D.; Que, L., Jr.; Collins, T. J.; Münck, E.; Bominaar, E. L. *Inorg. Chem.* **2008**, *47*, 3669–3678.
(13) Anastas, P. T. *Crit. Rev. Anal. Chem.* **1999**, *29*, 167–175.
(14) Ryabov, A. D.; Collins, T. J. *Adv. Inorg. Chem.* **2009**, *61*, 471–521.
(15) Popescu, D.-L.; Chanda, A.; Stadler, M. J.; Mondal, S.; Tehranchi, J.; Ryabov, A. D.; Collins, T. J. *J. Am. Chem. Soc.* **2008**, *130*, 12260–12261.
(16) Website: http://www.chem.cmu.edu/groups/collins/awardpatpub/patents/index.html.
(17) Ghosh, A. *Design, Synthesis and Mechanistic Studies of Iron–TAML Catalytic Activators of Hydrogen Peroxide and a New Activation Chemistry of Dioxygen by Iron*; Carnegie Mellon University: Pittsburgh, PA, 2004.
(18) George, P. *Biochem. J.* **1953**, *54*, 267–276.

dilutions of this acidic stock solution were made daily using 0.01 M phosphate buffer.

Job Method of Continuous Variation. Phosphate buffer (3 mL) was added to a quartz cuvette with a stopper. The total concentration of interacting species in the cuvette was kept constant at 1×10^{-4} M by mixing the appropriate concentrations of the stock solutions of **1a** and the oxidant. UV/vis spectroscopic data were collected in the range of 290−1100 nm. An aliquot of Fe^{III}−TAML solution was added to the cuvette, and a spectrum was recorded. Then, an aliquot of K_2IrCl_6 was added to the cuvette, and the next spectrum was run after 3 min which allowed the absorbance changes to plateau. The wavelength of 775 nm was used for data collection because the absorbance of **1a** is insignificant at this wavelength and that of K_2IrCl_6 is negligible at the concentrations used.

Determination of the Equilibrium Constants. Phosphate buffer (3 mL) was added to a quartz cuvette with a stopper. An aliquot of **1a** was added to obtain a concentration of 1.2×10^{-4} M in the cuvette. Aliquots of the oxidant (3×10^{-5} M) were added to the solution. After each addition of the oxidant, the absorbance was allowed to reach a constant value.

Transient Kinetic Studies. Transient kinetic experiments were performed using a Bio-Logic stopped-flow spectrophotometer (model MOS-450/CD) equipped with a 2-syringe stopped-flow mixer (model μSFM-20) that utilizes a motor power supply model MPS-20. The experiments were run in the temperature range of 15−45 °C using a Neslab RTE-10 D1 circulating bath with a heater/cooler controlled by a digital thermometer with a precision of ±0.1 °C. The syringes in the stopped-flow apparatus were filled with solutions in 0.01 M phosphate or carbonate buffers, pH 6.0−13.8, and were allowed to equilibrate at the bath temperature for ∼15 min. The dead time of the instrument was 4 ms. A stopped-flow observation cell (model FC-15) had a 1.0 mm optical path length. The product formation was followed at 420 and 780 nm. Each kinetic trace used for calculating k_{obs} is an average of at least 5 runs. Pseudo-first-order rate constants (k_{obs}) were determined by fitting kinetic traces to the function $A = a_o e^{-kt} + b_o$, where k is k_{obs} in s^{-1}. Stopped-flow experiments at pressures up to 130 MPa were performed using a custom built instrument previously described.[19] The data at pH 8.0 and 10.8 were obtained using 0.02 M [tris(hydroxymethyl)-methyl]aminopropanesulfonic acid (TAPS) and (cyclohexylamino)-propanesulfonic acid (CAPS) buffer solutions, respectively. Variation of buffer concentration had no influence on the observed rate constants, which ruled out the possible role of organic buffers as substrates during the reaction with hydrogen peroxide. Kinetic traces were analyzed with OLIS KINFIT software (Bogart, GA, 1989). Reported rate constants are the mean values from at least five kinetic runs.

Results

UV/vis Studies of the Oxidation of 1 by H_2O_2 and K_2IrCl_6. Stoichiometry and Thermodynamics. Hydrogen peroxide reacts with **1** about 100 times faster than does ^{t}BuOOH.[6] There is a noticeable catalase-like activity of **1** with an excess of H_2O_2.[9] Previous kinetic studies of the catalyzed bleaching of Orange II have led us to conclude that H_2O_2 and ^{t}BuOOH react with **1** to produce a common intermediate.[6] Therefore, we anticipated that H_2O_2 and ^{t}BuOOH would transform **1** into species with similar spectra. Indeed, UV/vis spectra produced from **1e** with H_2O_2 in water (Figure 1) look the same as those derived from **1e** with ^{t}BuOOH (not shown). A significant increase in absorbance in the range of 350−550 nm was

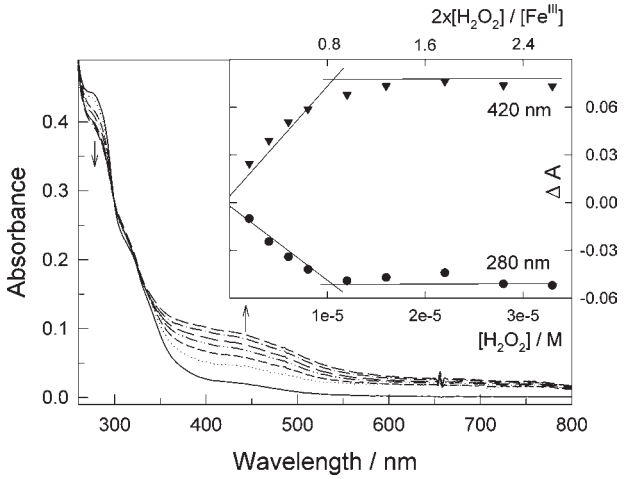

Figure 1. Spectral changes of **1e** (2.5×10^{-5} M) in the presence of 0, 2×10^{-6}, 4×10^{-6}, 6×10^{-6}, 8×10^{-6}, 12×10^{-6}, and 16×10^{-6} M H_2O_2 at pH 11.4, 25 °C. Arrows show dynamics of absorbance change. Inset: Titration curves at 280 (●) and 420 (▼) nm consistent with a 2:1 (Fe^{III}/H_2O_2) stoichiometry.

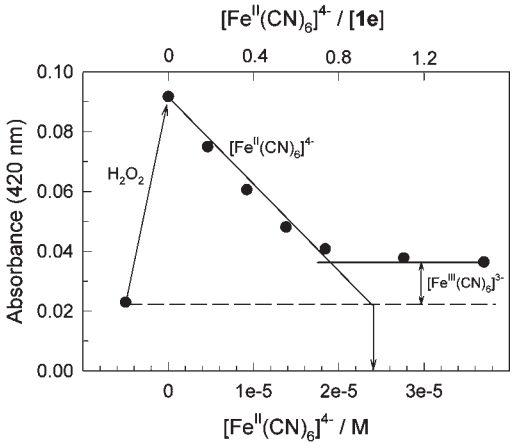

Figure 2. Titration of the intermediate generated from **1e** (2.5×10^{-5} M) and half-equivalent of H_2O_2 by $[Fe(CN)_6]^{4-}$ showing a 1:1 stoichiometry at pH 11.35, 0.1 M KPF_6, 25 °C.

produced by a less than stoichiometric amount of H_2O_2. The inset in Figure 1 shows the absorbance changes for specific wavelengths at pH 11.4 as a function of added [H_2O_2] which point to the reaction stoichiometry. Data obtained for both **1a** and **1e** indicate that the absorbing species are oxidized by 1 equiv above the ferric starting state to Fe^{IV} as was previously found with ^{t}BuOOH as the oxidant.[12] Similar studies performed for **1a** at pH 8.33 in the presence of 1.0 M $NaClO_4$ also indicate an iron(IV) product.

The oxidized species obtained from **1e** with a half equivalent of H_2O_2 was *reduced* back to the ferric state by 1 equiv of $[Fe^{II}(CN)_6]^{4-}$ (Figure 2). The absorbance did not reach the exact initial level at 420 nm because the oxidized titrant $[Fe^{III}(CN)_6]^{3-}$ absorbs light at this wavelength. Iron(IV) could also be generated from **1** and $[Ir^{IV}Cl_6]^{2-}$, a strong oxidizing agent that has been used for making Compounds I and II from the resting state of horseradish peroxidase.[20,21] $[Ir^{IV}Cl_6]^{2-}$ induced similar

(19) van Eldik, R.; Gaede, W.; Wieland, S.; Kraft, J.; Spitzer, M.; Palmer, D. A. *Rev. Sci. Instrum.* **1993**, *64*, 1355–1357.

(20) Hayashi, Y.; Yamazaki, I. *J. Biol. Chem.* **1979**, *254*, 9101–9106.

(21) Chouchane, S.; Lippai, I.; Magliozzo, R. S. *Biochemistry* **2000**, *39*, 9975–9983.

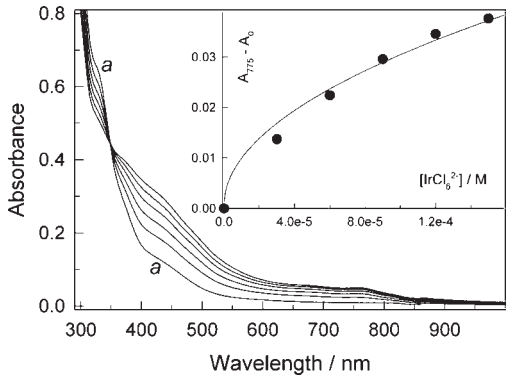

Figure 3. Spectra of complex **1a** (1.2×10^{-4} M) in the absence (*a*) and in the presence of (1.2, 3, 6, 9, 12, and 15) $\times 10^{-4}$ M $[Ir^{IV}Cl_6]^{2-}$. Inset shows absorbance changes at 775 nm induced by different concentrations of $[Ir^{IV}Cl_6]^{2-}$; the solid line is the calculated changes using the best fit values of K_1 and $\Delta\varepsilon$ of eq 2 (see text for details). Conditions: pH 11, 25 °C.

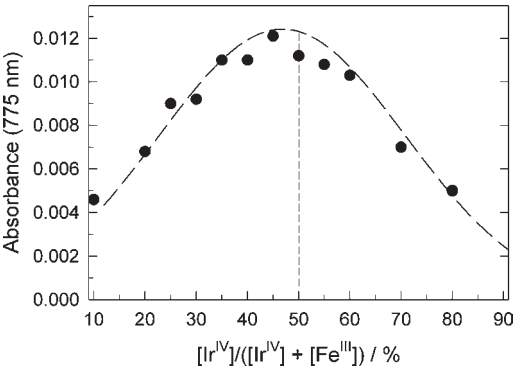

Figure 4. Job plot illustrating a 1:1 molar ratio on interaction between complex **1a** and $[Ir^{IV}Cl_6]^{2-}$. Conditions: total concentration [**1a**] + $[Ir^{IV}]$ 1.0×10^{-4} M, pH 11, 25 °C.

spectral changes to H_2O_2 (Figure 3). The isosbestic point at 349 nm indicates the presence of two absorbing species, one of which is a monomeric form of iron(IV), such as **3**, in a dilute solution (around 10^{-4} M) at pH 11. Therefore, the Job method of continuous variation[22,23] could be used to explore the redox stoichiometry of the oxidation of **1**.

The Job plot in Figure 4 confirms that **1a** and Ir^{IV} react in a 1:1 molar ratio and the interaction between **1** and $[Ir^{IV}Cl_6]^{2-}$ follows eq 1. The Job plot for the interaction between **1** and H_2O_2 (Supporting Information, Figure S1) exhibits a maximum absorbance at $[H_2O_2]/([H_2O_2]+[Fe^{III}]) \approx 0.33$, in accordance with the 2:1 (Fe^{III}/H_2O_2) stoichiometry. The effective equilibrium constant K_1 can be estimated from the data in Figure 3.

$$Fe^{III} + Ir^{IV} \rightleftharpoons Fe^{IV} + Ir^{III} \qquad K_1 = \frac{[Fe^{IV}][Ir^{III}]}{[Fe^{III}][Ir^{IV}]} \quad (1)$$

Then, using the known reduction potential for the half-reaction $[Ir^{IV}Cl_6]^{2-} + e^- \rightarrow [Ir^{III}Cl_6]^{3-}$,[24] the reduction potential for the half-reaction $[Fe^{IV}L(=O)(OH_2)]^{2-} + e^- + H_2O \rightarrow [Fe^{III}L(OH)(OH_2)]^{2-} + OH^-$ can be calculated. The data in Figure 3 was collected using comparable concentrations of **1a** and Ir^{IV}. Under such conditions, a dependence of $A_{775} - A_o$ on total concentrations Ir_t and Fe_t is given by eq 2 (for details, see Supporting Information).

$$A_{775} - A_0 = \Delta\varepsilon \frac{(Ir_t + Fe_t) - \sqrt{(Ir_t+Fe_t)^2 - 4\left(1 - \frac{1}{K_1}\right)(Ir_tFe_t)}}{2\left(1 - \frac{1}{K_1}\right)} \quad (2)$$

Fitting the experimental data in Figure 3 obtained at pH 11 (water is oxidized by Ir^{IV} at higher pH[25]) to eq 2 gives $K_1 = 1.0005 \pm 0.0030$. Since $RT \ln K_1 = -nF\Delta E$ (F is the Faraday constant, $\Delta E = E(Ir^{III}/Ir^{IV}) - E(Fe^{III}/Fe^{IV})$[26] and $K_1 \sim 1$, the $E(Fe^{III}OH/Fe^{IV}O)$ reduction potential equals that of the Ir^{III}/Ir^{IV} couple (0.87 V versus NHE[24]).

Electrochemical Studies of 1a at pH 12.6. Compounds **1** show reversible or quasi-reversible electrochemical behavior at electrodes in acetonitrile when the cyclic voltammetry technique is applied.[9] The scenario changes significantly in water where there is only one known example of the reversible electrochemistry for a non-heme oxoiron(IV) complex.[27] For different **1**, broad, irreversible, and poorly reproducible cyclic voltammograms have been obtained in water. Recent work has suggested reasons for the poor reversibility.[12] Electrooxidation of **1** in water might generate reactive Fe^{IV} (and perhaps Fe^{V} derivatives). Under slightly acidic to slightly basic conditions Fe^{IV}-μ-oxo dimers are formed. At higher pH, **3** is formed. Therefore, a set of iron species may be produced depending on the pH.[12] Moreover, electrochemical formation of Fe^{IV}-oxo or μ-oxo species in water occurs presumably via a proton-coupled electron transfer mechanism (PCET).[28] Consequently, pH 12.6 was chosen for electrochemical studies of **1a** to minimize the complexity because Fe^{IV} is the monomeric species **3** at this pH (Scheme 1).

First-scan cyclic voltammograms of **1a** are irreversible, and their shapes are significantly affected by the scan rate (Figure 5A). The voltammogram measured at a scan rate of 2 mV s^{-1} has a peak at 0.88 V and two shoulders at about 0.8 and 1.0 V versus SCE. At a scan rate of 20 mV s^{-1} one broad irreversible peak is observed at 1.1 V. Multiple peaks and a drift in the peak potential by 0.3 V with increasing scan rate implicate multiple equilibria among the iron species and show that data in Figure 5A are poorly informative. Therefore, differential pulse voltammetry[29] was applied. The data in Figure 5B show two peaks at 0.66 and 0.86 V (versus SCE). The potential of the first peak (0.66 V vs SCE or 0.90 V vs NHE) is particularly close to the estimated reduction potential for the Fe^{III}/Fe^{IV} couple (0.87 V vs NHE) obtained in the

(22) Job, P. *Ann. Chim. Appl.* **1928**, *9*, 113–203.
(23) Job, P. *C. R.* **1925**, *180*, 928–930.
(24) Lide, D. R., *CRC Handbook of Chemistry and Physics*, 87th ed.; CRC Taylor & Francis: New York, 2006−2007.
(25) Fine, D. A. *Inorg. Chem.* **1969**, *8*, 1014–1016.
(26) Bard, A. J.; Faulkner, L. R. *Electrochemical Methods. Fundamentals and Applications*; John Wiley & Sons: New York, 1980.
(27) Wang, D.; Zhang, M.; Buhlmann, P.; Que, L., Jr. *J. Am. Chem. Soc.* **2010**, *132*, 7638–7644.
(28) Costentin, C. *Chem. Rev.* **2008**, *108*, 2145–2179.
(29) Wang, J. *Analytical Electrochemistry*; Wiley-VCH: Hoboken, NJ, 2006.

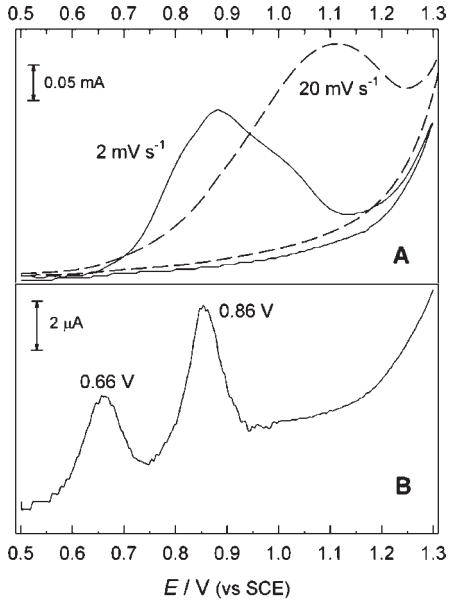

Figure 5. (**A**) Cyclic voltammograms of **1a** (0.001 M) in aqueous KOH solution (pH 12.6) at scan rates 2 and 20 mV s^{-1}. (**B**) Differential pulse voltammograms of the same sample under the same conditions obtained at a step potential of 0.001 V, modulation amplitude 0.015 V, and scan rate 2 mV s^{-1}. Subtraction of the background signal was applied.

titration experiment (see above). Therefore, the first peak in Figure 5B could be tentatively assigned to the same phenomenon. The second peak assignment at 0.86 V versus SCE is less certain. It is tempting to speculate that the peak arises from an unstable Fe^{V} species, similar to compound **2**, especially given the characterization of **2** in non-coordinating solvents at −60 °C (Scheme 1).

Transient Kinetic Studies of Reactions between 1 and ^{t}BuOOH. As noted above, **1** displays catalase-like activity in an excess of H_2O_2 in the absence of electron donors. This complicates stopped-flow kinetic studies of the interaction between **1** and H_2O_2. Reliable measurements with H_2O_2 were possible under a limited set of conditions. Most of the kinetic data for the formation of **3** and **4** were collected using ^{t}BuOOH. Under pseudo-first-order conditions, that is, at least a 10-fold excess of ^{t}BuOOH, the spectral pattern stabilizes in a matter of 1−2 s. The spectra generated using ^{t}BuOOH are longer lived (ca. 30 min) than in the case of H_2O_2, which are stable for ∼10 min only if the catalyst to peroxide molar ratio is around 1:1. If an excess of H_2O_2 is used, the new spectroscopic bands vanish in a matter of seconds depending on the pH. The interaction between **1a** and an excess of ^{t}BuOOH is virtually irreversible under pseudo-first order conditions suggested by the independence found for the product absorbance at 780 nm on [^{t}BuOOH] in the concentration range employed.

Stopped-flow kinetic data were collected at 420 and 780 nm ([**1a**] = 3.0×10^{-5} M, [^{t}BuOOH] = $(0.031-3.6) \times 10^{-2}$ M) at 17, 25, and 35 °C. A typical trace obtained at 420 nm is shown as an average of five runs in the inset in Supporting Information, Figure S2. The observed pseudo-first-order rate constants (k_{obs}) measured at the two wavelengths were close. Other kinetic models were tested (biexponential, second order), but did not give better fits. Plots of k_{obs} as a function of [^{t}BuOOH] were linear (e.g., Supporting Information, Figure S2) indicating a first-order

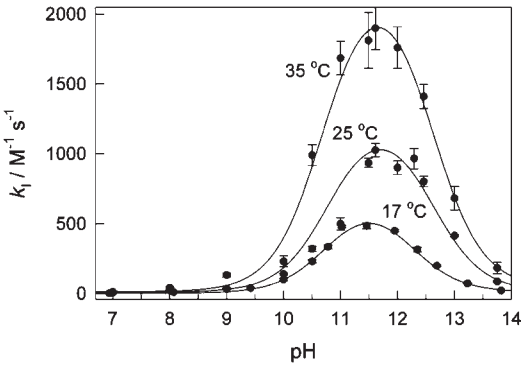

Figure 6. pH profiles for the rate constants k_I for the reaction of **1a** with ^{t}BuOOH at 17, 25, and 35 °C, 0.01 M phosphate.

Scheme 2. Stoichiometric Mechanism of Oxidation of Fe^{III}−TAML Activators **1** by Peroxides in Aqueous Solution That Accounts for the pH Dependencies of k_I

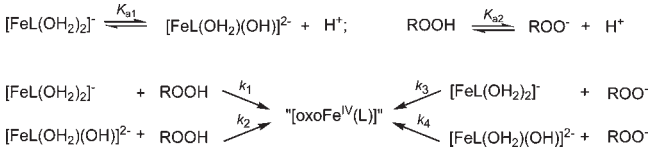

dependence in peroxide ($k_{obs} = k_I$[peroxide]). The intercepts were insignificant pointing to the irreversibility of the reaction. The conditional second-order rate constants k_I for **1a** are strongly pH dependent (Figure 6). There are sharp maxima at pH around 11.5 at all three temperatures.

The pH profile in Figure 6 is rationalized in terms of the mechanism in Scheme 2, which has been proposed on the basis of kinetic data obtained under the steady-state conditions.[9,15] It assumes that complexes **1** are six-coordinate in water with the two axial sites being occupied by H_2O. One aqua ligand undergoes reversible deprotonation with pK_{a1} around 10.5 for **1a**.[30] The pK_{a2} for ^{t}BuOOH is 12.4 ± 0.2.[31] The species generated in two acid−base equilibria react pair wise (Scheme 2). The k_2 and k_3 pathways are kinetically indistinguishable. The mechanism in Scheme 2 leads to eq 3 that can be used to rationalize the pH profiles such as shown in Figure 6.

$$k_I = \frac{k_1[H^+]^2 + (k_2K_{a1} + k_3K_{a2})[H^+] + k_4K_{a1}K_{a2}}{[H^+]^2 + (K_{a1} + K_{a2})[H^+] + K_{a1}K_{a2}} \quad (3)$$

The data in Figure 6 have been fitted to eq 3 for the estimation of the intrinsic equilibrium and rate constants summarized in Table 1. The kinetically indistinguishable rate constants k_2 and k_3 were calculated by assuming that one of the two rate constants is zero. The solid lines in Figure 6 are calculated curves using the data in Table 1 under the assumption that k_3 (or k_2) is negligible. There is an agreement between the experimental and calculated data. The data obtained for **1a** at different temperatures (Table 1) have been used for calculating the activation ($\Delta H^{\ddagger}$, $\Delta S^{\ddagger}$) and thermodynamic ($\Delta H°$ and $\Delta S°$) parameters, which are summarized in Table 2.

(30) Ghosh, A.; Ryabov, A. D.; Mayer, S. M.; Horner, D. C.; Prasuhn, D. E., Jr.; Sen Gupta, S.; Vuocolo, L.; Culver, C.; Hendrich, M. P.; Rickard, C. E. F.; Norman, R. E.; Horwitz, C. P.; Collins, T. J. *J. Am. Chem. Soc.* **2003**, *125*, 12378–12378.
(31) Davies, G.; Garafalo, A. R. *Inorg. Chem.* **1976**, *15*, 1101–1106.

Table 1. Calculated Rate Constants (in $M^{-1} s^{-1}$) and pK_a Values for the Reactions between **1** and ^{t}BuOOH as Indicated in Scheme *2* in 0.01 M Phosphate Buffer (K^+ salt) Obtained by Fitting Experimental Data Such as in Figure *6* to eq *3*

complex	T/°C	k_1	$10^{-3} \times k_2$	$10^{-3} \times k_3$	k_4	pK_{a1}	pK_{a2}
1a	15[a]	70.0 ± 0.2	20.0 ± 0.5	160 ± 3	10.0 ± 0.1	10.6 ± 0.1	11.5 ± 0.2
	17	2.0 ± 0.3	0.72 ± 0.05	18 ± 1	10.0 ± 0.5	10.8 ± 0.1	12.2 ± 0.3
	25	10.0 ± 0.2	1.3 ± 0.2	83 ± 3	15 ± 1	10.8 ± 0.1	12.6 ± 0.2
	35	13 ± 1	2.4 ± 0.5	190 ± 5	38 ± 3	10.7 ± 0.1	12.6 ± 0.4
	25[b]	45 ± 2	1.8 ± 0.4	135 ± 13	20 ± 1	10.6 ± 0.1	12.1 ± 0.1
	25[c]	12.0 ± 0.5	2.0 ± 0.1	200 ± 2	5.0 ± 0.2	10.5 ± 0.1	12.5 ± 0.2
1b	25	10.0 ± 0.5	1.10 ± 0.03	28 ± 4	38 ± 2	11.0 ± 0.3	12.4 ± 0.1
1c	25	30 ± 2	0.95 ± 0.03	380 ± 4	35 ± 3	9.9 ± 0.1	12.5 ± 0.2
1d	25	10.0 ± 0.3	1.25 ± 0.05	620 ± 1	15 ± 1	9.9 ± 0.2	12.6 ± 0.4

[a] With H_2O_2. [b] In 0.01 M carbonate buffer. [c] In 0.01 M phosphate buffer, sodium salt.

Table 2. Activation and Thermodynamic Parameters for the Interaction between **1a** and ^{t}BuOOH in 0.01 M Phosphate Buffer

parameter	$\Delta H^{\ddagger}$ or $\Delta H°$/kJ mol^{-1}	$\Delta S^{\ddagger}$ or $\Delta S°$/J K mol^{-1}
k_1	73 ± 1	15 ± 2
k_2	46.3 ± 0.3	−31.9 ± 0.1
k_3	93.8 ± 0.3	161 ± 13
k_4	53.1 ± 0.1	−43.6 ± 0.5
K_{a1}	10 ± 5	−170 ± 20
K_{a2}	−36 ± 24	−360 ± 80

The measurements have been performed for Fe^{III}−TAML activators **1a**−**d** with different substituents on the aromatic ring of the molecule. Similar kinetics holds through the series of catalysts. Bell-shaped pH profiles similar to those in Figure 6 were observed, and the corresponding data were fitted to eq 3. The best-fit values for the rate and equilibrium constants are summarized in Table 1. The kinetic data described above were collected in a phosphate buffer solution. The buffer ion $H_2PO_4^-$ is known to behave as a general acid catalyst in the demetalation of **1**.[32] While the demetalation time scale is much larger than that associated with peroxide activation (k_I), similar measurements have been performed in carbonate buffer which is less active as a demetalating buffer ion. The results in Figure 7 demonstrate a slight increase in k_I together with a half-unit shift to lower pH of the bell-shaped curve in the carbonate versus phosphate buffer. The shift is partly due to a decrease in pK_{a1} in the carbonate buffer (Table 1), the molecular origin of which is unknown at this time.

The pK_{a1} values for different Fe^{III}−TAMLs in Table 1 agree with the values measured directly by UV/vis spectroscopy.[30] The pK_{a1}'s determine the left side of the bell-shaped dependence such as in Figure 6. The right side is primarily affected by the pK_{a2} of ^{t}BuOOH. The pK_a of H_2O_2 is lower than that of ^{t}BuOOH by about one unit. Therefore, if the mechanism in Scheme 2 is correct, the pH profile for k_I using H_2O_2 should be sharper and the right side should be shifted to neutral pH. To test this, we have searched for conditions that would allow the kinetics of reaction between **1a** and hydrogen peroxide to be accurately measured by the stopped-flow technique.

Kinetics of Reaction between 1a and H_2O_2. At 15 °C, satisfactory exponential kinetic traces were obtained over the entire pH range (7−13.5) with k_{obs} corresponding to the formation from **1a** and H_2O_2 of **3** or **4** depending on pH.

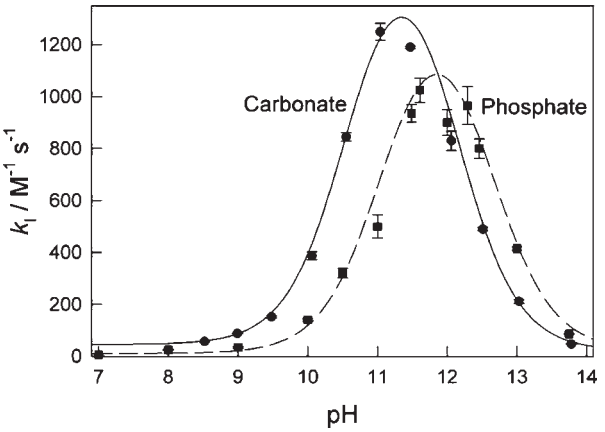

Figure 7. pH profiles for the rate constants k_I for the reaction of **1a** with ^{t}BuOOH in 0.01 M carbonate buffer (●) and 0.01 M phosphate buffer (■) at 25 °C.

At 20 °C and above, satisfactory data were available at pH below 10. The entire pH range could not be covered. As in the ^{t}BuOOH case, the values of k_{obs} were proportional to the concentration of H_2O_2 in the range (0.36−8.4) × 10^{-3} M (see Supporting Information, Figure S3). First-order kinetics in H_2O_2 was also confirmed by a careful analysis of the initial rates measured at different [H_2O_2]. The rate constants k_I were calculated from the slopes of the linear plots and are shown as a function of pH in Figure 8. The data were fitted to eq 3 and the best-fit values are included in Table 1. The value of pK_{a1} agrees with that obtained for the reaction with ^{t}BuOOH (this work) and measured independently elsewhere.[30] The intrinsic rate constants k_1−k_4 are larger for H_2O_2 than for ^{t}BuOOH as was found in previous work.[6]

Kinetics of Reaction between 1a and H_2O_2 at Elevated Pressure. The effect of pressure on the reaction between **1a** and H_2O_2 was studied at pH 8.0 and 10.8. Under these conditions, **1a** exists predominantly as $[FeL(OH_2)_2]^-$ and $[FeL(OH_2)OH)]^{2-}$, respectively, though the dominant form of hydrogen peroxide is H_2O_2. Measurements at pH 10.8 were performed at 3 °C to minimize the catalase-like activity of **1a**. The data shown in Figure 9 indicate that a change in the speciation of **1a** noticeably affects the pressure dependence, that is, increasing pressure accelerates the reaction at pH 8.0, but decelerates it at pH 10.8. Thus, the reaction of **1a** with H_2O_2 has features of an associative process at lower pH ($\Delta V^{\ddagger} = -7$ cm^3 mol^{-1}) but seems to be more dissociative under more basic conditions ($\Delta V^{\ddagger} = +2$ cm^3 mol^{-1}).

(32) Polshin, V.; Popescu, D.-L.; Fischer, A.; Chanda, A.; Horner, D. C.; Beach, E. S.; Henry, J.; Qian, Y.-L.; Horwitz, C. P.; Lente, G.; Fabian, I.; Münck, E.; Bominaar, E. L.; Ryabov, A. D.; Collins, T. J. *J. Am. Chem. Soc.* **2008**, *130*, 4497–4506.

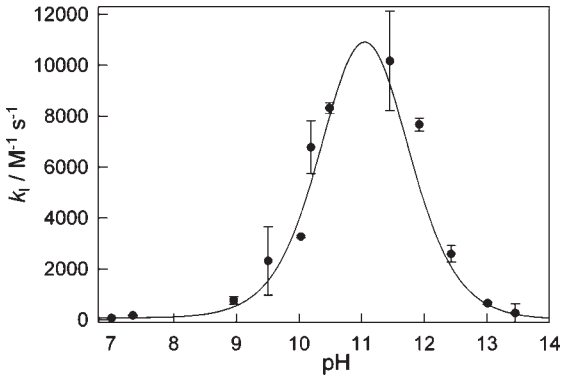

Figure 8. Dependence of k_1 on pH for the reaction of **1a** with H_2O_2 in 0.01 M phosphate at 15 °C.

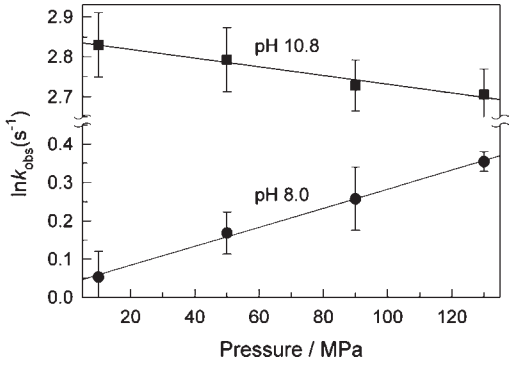

Figure 9. Pressure dependencies of the rate (ln k_{obs}) of reaction of **1a** with H_2O_2 at pH 8.0 (●) and 10.8 (■). Conditions: [**1a**] 1×10^{-4} M, [H_2O_2] 1×10^{-3} M, 0.1 M $NaClO_4$; pH 8: 0.02 M TAPS buffer, 25.5 °C, pH 10.8: [**1a**] 5×10^{-5} M, [H_2O_2] 5×10^{-4} M, 0.1 M $NaClO_4$, 0.02 M CAPS buffer, 3 °C.

Discussion

General Comments. The kinetic results presented here on the oxidation of **1** by H_2O_2 match those reported on the **1**-catalyzed steady-state oxidation by H_2O_2 of the reactive cyclometalated Ru^{II} electron donor [Ru^{II}(*o*-C_6H_4py)-(phen)$_2$]PF_6.[9] The rate was found to be independent of Ru^{II} concentration at pH 6−12.4 in accordance with a rate-limiting interaction between **1** and H_2O_2. Moreover, similarities among the kinetic data reported both here and previously[9] are underscored by the bell-shaped pH profile (Figure 8) and the matching rate and equilibrium constants (Table 1) calculated in terms of the mechanism in Scheme 2 and eq 3. The information acquired using ^{t}BuOOH lends additional support to the proposed mechanism. The pH maxima for the rate constant k_1 measured for H_2O_2 and ^{t}BuOOH (Figures 8 and 6, respectively) are not identical. There is a shift to more basic pH for ^{t}BuOOH. The mechanism in Scheme 2 accounts for this phenomenon because the pK_a of ^{t}BuOOH is about one pH unit less acidic than that of H_2O_2.[31]

Despite a significant mechanistic interest for interactions of iron non-heme compounds with O_2 and H_2O_2, the primary biological oxidants, information regarding monomeric Fe^{III} complexes and H_2O_2 to afford iron species in higher oxidation states in aqueous solutions is limited.[33] This is surprising in view of the fact that such reactions are key steps in catalysis by peroxidase enzymes[34] and in the "peroxide shunt" found for catalysis by cytochrome P450.[35,36] There is a detailed study of the reaction of [Fe^{III}(EDTA)H_2O]$^-$ with H_2O_2, but the end-product is a monomeric iron(III) peroxo species.[37] Iron(III) complexes of 1,4,8,11-tetraaza[14]annulenes activate H_2O_2 in catalase-like processes with rate constants of 1400−2400 M^{-1} s^{-1} at pH 7.[38] As for the Fe^{III}−TAML case, an aqua/hydroxo complex [FeL(OH)(H_2O)] is viewed as the most reactive species interacting with H_2O_2. A reactivity−pH profile with a maximum at 11 similar to that in Figure 8 is known for the [iron(III) (octaphenylsulfonato)-porphyrazine]$^{5-}$ catalyzed bleaching of Orange II by H_2O_2.[39] An aqua/hydroxo iron(III) species and HO_2^- comprise the most reactive couple. More straightforward comparisons of the reactivity of **1** and H_2O_2 invoke examples from the chemistry of porphyrins. Peroxidase activity of the hemeoctapeptide *N*-acetylmicroperoxidase-8, where the active site is composed of an iron(III) aqua complex with histidine as second axial ligand, is characterized by a maximum activity again at pH around 10.[40] In contrast to the mechanism in Scheme 2, the highest reactivity is ascribed to the couple Fe^{III}−H_2O and HO_2^-. Deprotonation of the aqua ligand leads to unreactive species. In the case of **1**, a similar deprotonation increases the reactivity, and we propose that the activation results from a labilization of the aqua ligand *trans* to hydroxide. It is interesting to note that there is no maximum on the pH profile of a similar reaction between iron(III) complexed to 5,10,15,20-tetrakis(2,6-dimethyl-3-sulfonatophenyl)porphyrin and H_2O_2.[41] The reaction rate increases with increasing pH in the range of 1−12, and the highest reactivity is ascribed to the [Fe^{III}L(OH)-(H_2O)]$^{4-}$/HO_2^- couple. Thus, the behavior of the first generation Fe^{III}−TAML complexes **1** toward H_2O_2 is closer to that of [Fe^{III}(EDTA)H_2O]$^-$ than to Fe^{III} complexes with porphyrin type ligands.

Mechanism of Formation of Fe^{IV}−TAMLs. The majority of Fe^{III}−TAML oxidative processes do not appear to involve dominating free radical chemistry.[14] Therefore, a one electron oxidation of **1** by either H_2O_2 or ^{t}BuOOH into **3** or **4** is highly improbable. We have previously argued that the Fe^{III}−TAML oxidative chemistry has much in common with catalysis by peroxidase enzymes[9] and established the formation of an Fe^{V}−TAML-oxo species in non-aqueous medium by spectroscopic techniques.[10] Consequently, it is reasonable to propose that peroxides are capable of transforming **1** into an Fe^{V} form in water. Iron(V) species have not yet been detected in water by spectroscopic methods. Therefore, it can be

(33) Kryatov, S. V.; Rybak-Akimova, E. V.; Schindler, S. *Chem. Rev.* **2005**, *105*, 2175–2226.
(34) Dunford, H. B. *Heme Peroxidases*; Wiley-VCH: New York, 1999.
(35) Sono, M.; Roach, M. P.; Coulter, E. D.; Dawson, J. H. *Chem. Rev.* **1996**, *96*, 2841–2887.
(36) Meunier, B.; de Visser, S. P.; Shaik, S. *Chem. Rev.* **2004**, *104*, 3947–3980.
(37) Brausam, A.; van Eldik, R. *Inorg. Chem.* **2004**, *43*, 5351–5359.
(38) Sustmann, R.; Korth, H.-G.; Kobus, D.; Baute, J.; Seiffert, K.-H.; Verheggen, E.; Bill, E.; Kirsch, M.; de Groot, H. *Inorg. Chem.* **2007**, *46*, 11416–11430.
(39) Theodoridis, A.; Maigut, J.; Puchta, R.; Kudrik, E. V.; van Eldik, R. *Inorg. Chem.* **2008**, *47*, 2994–3013.
(40) Marques, H. M. *Inorg. Chem.* **2005**, *44*, 6146–6148.
(41) Zipplies, M. F.; Lee, W. A.; Bruice, T. C. *J. Am. Chem. Soc.* **1986**, *108*, 4433–4445.

Scheme 3. More Extensive Picture of the *Stepwise* Mechanistic Events Proposed to Play a Role in the k_1, k_2, and k_3 Pathways for the Formation of an Iron(V)oxo Intermediate

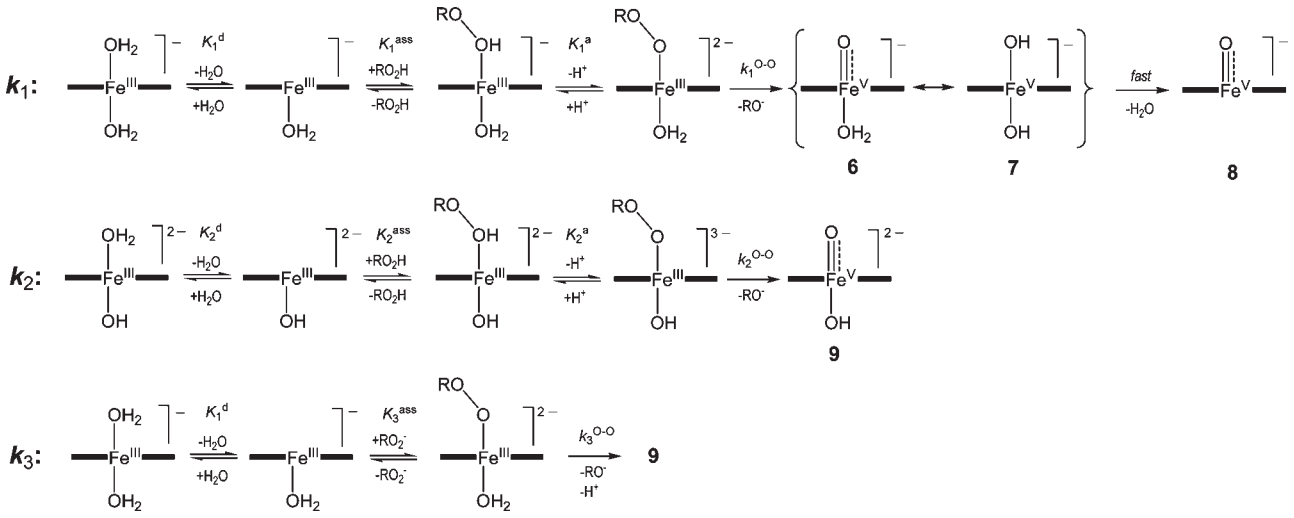

assumed that iron(V), once formed, is rapidly converted into iron(IV) species. In analogy with the chemistry of porphyrins,[42−44] the rapid comproportionation of Fe^{III} and Fe^{V} species is suggested. Fe^{IV}−TAML complexes do not seem to react with peroxides in water to form detectable higher oxidized state complexes and Fe^{IV} species appear as the final products formed in this solvent.

The mechanisms of formation of Fe^{V} species under the action of dibenzoyl peroxide[6] and hydrogen peroxide[9] have been discussed. The new data support the conclusions of both prior studies and a predominant heterolytic mechanism for ^{t}BuOOH activation. The O−O bonds of alkylhydroperoxides are cleaved via both homolytic and heterolytic mechanisms.[45−48] Our previous studies indicated that H_2O_2 and ^{t}BuOOH behave similarly in oxidation reactions[6,49]—heterolysis of ^{t}BuOOH is more likely in the presence of Fe^{III}−TAMLs. The k_1 and k_2 pathways in Scheme 3 contain extra details of the *stepwise* mechanism.[9] The mechanism involves the binding peroxide ROOH (K^{d} K^{ass}) to iron(III), deprotonation (K^{a}), and the rate-limiting heterolysis of the O−O bond (k^{O-O}).

The rate constants k_1−k_3 summarized in Table 1 are products of the corresponding equilibrium and rate constants, that is, $k_i = K_i^{d} K_i^{ass} K_i^{a} k_i^{O-O}$ (i = 1, 2) or $k_3 = K_1^{d} K_3^{ass} k_3^{O-O}$. The equilibria in the expressions for k_1−k_3 that precede the slowest step must be shifted to the left. Otherwise the observed first order dependence in peroxide would not hold. The arguments for excluding the mechanistic option entailing rate-limiting coordination of ROOH to Fe^{III} have been formulated previously.[9] Structures of complexes **6**−**9** in Scheme 3 are tentative because the speciation of the iron(V) in water is unknown. Structure **7**, a tautomeric form of **6**, is invoked by analogy with those recently postulated for compound II of haloperoxidases.[50,51]

Replacement of water by peroxide and peroxo anion is displayed as a dissociative process in Scheme 3. Compounds such as **1** have axial Lewis acidity that is muted by the powerful tetra-anionic equatorial TAML system resulting in a limited affinity for the sixth axial ligand and do exist as five-coordinate species in the solid state.[14] This hypothesis might be particularly true for the k_2 pathway because of the increased trans influence of the OH^{-} anion. In fact, a dissociative interchange I_d mechanism may be operative. This would lead to a more compact Scheme 3. The mechanism in Scheme 3 shrinks further assuming a proton-coupled electron transfer mechanism for the cleavage of the peroxide O−O. Recognition of the importance of PCET mechanisms in chemistry and biochemistry has grown significantly in the last two decades.[28,52−54] Substantial evidence supports a PCET mechanism in the O−O bond cleavage of hydrogen peroxide by peroxidase enzymes.[54] Assuming that the I_d and PCET mechanisms are operative here, Scheme 3 can be rewritten as Scheme 4, which is advantageous for interpreting the pressure effects measured in this work.

Pressure Effects for the k_1 and k_2(k_3) Pathways. The interpretation of kinetic pressure effects of multistep chemical processes is a difficult task.[55−58] Scheme 4 shows

(42) Hodges, G. R.; Lindsay Smith, J. R.; Oakes, J. *J. Chem. Soc., Perkin Trans. 2* **1998**, 617–628.
(43) Hodges, G. R.; Lindsay Smith, J. R.; Oakes, J. *J. Chem. Soc., Perkin Trans. 2* **1999**, 1943–1952.
(44) Franke, A.; Wolak, M.; van Eldik, R. *Chem.—Eur. J.* **2009**, *15*, 10182–10198.
(45) Almarsson, O.; Bruice, T. C. *J. Am. Chem. Soc.* **1995**, *117*, 4533–4544.
(46) Belikova, N. A.; Tyurina, Y. Y.; Borisenko, G.; Tyurin, V.; Samhan-Arias, A. K.; Yanamala, N.; Furtmuller, P. G.; Klein-Seetharaman, J.; Obinger, C.; Kagan, V. E. *J. Am. Chem. Soc.* **2009**, *131*, 11288–11289.
(47) Labeque, R.; Marnett, L. J. *J. Am. Chem. Soc.* **1989**, *111*, 6621–6627.
(48) Nam, W.; Han, H. J.; Oh, S.-Y.; Lee, Y. J.; Choi, M.-H.; Han, S.-Y.; Kim, C.; Woo, S. K.; Shin, W. *J. Am. Chem. Soc.* **2000**, *122*, 8677–8684.
(49) Banerjee, D.; Apollo, F. M.; Ryabov, A. D.; Collins, T. J. *Chem.—Eur. J.* **2009**, *15*, 10199–10209.
(50) Stone, K. L.; Hoffart, L. M.; Behan, R. K.; Krebs, C.; Green, M. T. *J. Am. Chem. Soc.* **2006**, *128*, 6147–6153.
(51) Terner, J.; Palaniappan, V.; Gold, A.; Weiss, R.; Fitzgerald, M. M.; Sullivan, A. M.; Hosten, C. M. *J. Inorg. Biochem.* **2006**, *100*, 480–501.
(52) Thorp, H. H. *Chemtracts: Inorg. Chem.* **1991**, *3*, 171–184.
(53) Slattery, S. J.; Blaho, J. K.; Lehnes, J.; Goldsby, K. A. *Coord. Chem. Rev.* **1998**, *174*, 391–416.
(54) Huynh, M. H. V.; Meyer, T. J. *Chem. Rev.* **2007**, *107*, 5004–5064.
(55) van Eldik, R.; Hubbard, C. D., Application of high pressure in inorganic and bioinorganic chemistry. In *Chemistry at Extreme Conditions*; Riad Manaa, M., Ed.; Elsevier: Amsterdam, 2005; pp 109−164.
(56) van Eldik, R.; Hubbard, C. D. *Adv. Phys. Org. Chem.* **2006**, *41*, 1–78.
(57) Hubbard, C. D.; van Eldik, R. *Inorg. Chim. Acta* **2010**, *363*, 2357–2374.
(58) Hubbard, C. D.; van Eldik, R. *Physical Inorganic Chemistry. Methods and Techniques*; Bakač, A., Ed.; Wiley: New York, 2010; pp 269−365.

Scheme 4. Reduced Version of the Mechanism in Scheme *3* Based on the Assumption of the I_d and PCET Mechanisms (See Text for Details)

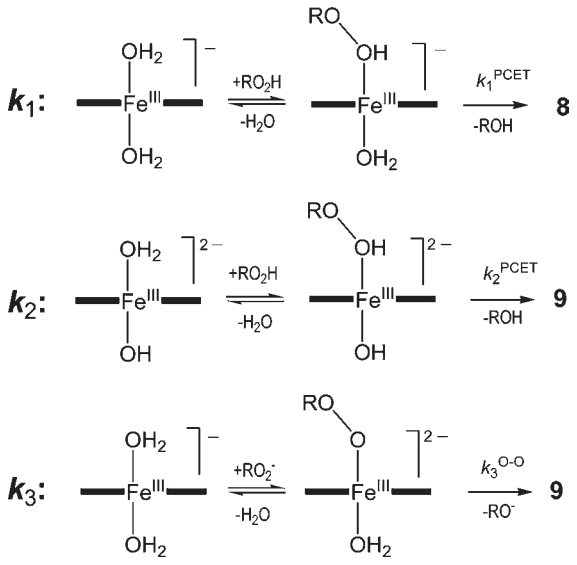

a two-step activation of peroxides by **1** involving pre-equilibrium binding followed by rate-limiting O−O bond cleavage. The partial molar volume of H_2O_2 exceeds that of H_2O and therefore a pressure increase should slightly favor the formation of the iron(III)-peroxide intermediate. The O−O bond cleavage might have features of a dissociative process though this is an oversimplification taking into account that the iron increases in oxidation state by two units. However, it can be argued that the overall charge of the iron complexes in the k_1 and k_2 pathways does not change and therefore a volume variation due to "an iron contribution" of the intermediates would be insignificant.[59] The effective volumes of activation $\Delta V^{\ddagger}$ were measured at pH 8.0 and 10.8 (Figure 9), where the k_1 and k_2 pathways dominate, respectively. Hence, we assign $\Delta V^{\ddagger}$ at pH 8.0 and 10.8 to the k_1 (-7 cm^3 mol^{-1}) and k_2 ($+2$ cm^3 mol^{-1}) pathways, respectively. The activation volume becomes more positive on going from the k_1 to the k_2 pathways. Thus, a dissociative process plays a more significant role for k_2 though associative features dominate for k_1. Axial ligands in the k_1 and k_2 pathways are H_2O and OH^-, respectively. Thus, binding of H_2O_2 to Fe^{III} might be more facile in the latter pathway because of the trans labilizing phenomenon of the hydroxo ligand.[60] The elongation of the O−O bond in the transition state contributes a volume increase that partially compensates the volume decrease caused by the binding of peroxide, which is likely the dominating feature for the k_1 pathway. Note that the O−O bond scission in the k_2 pathway occurs within an intermediate with the hydroxo ligand in the *trans* position as opposed to water in the k_1 pathway. The former pathway is significantly faster than the latter (Table 1), and this suggests that the OH^- ligand could play a role similar to that of coordinated cysteinate in catalysis by the P450 family of enzymes, where the O−O bond cleavage of

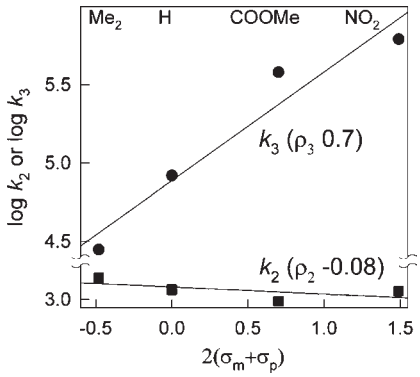

Figure 10. Hammett plots for the rate constants k_2 and k_3. The effective Hammett constant $2(m + p)$ reflects two channels by which the electronic effect from the head-ring substituents is delivered to the central metal (shown by arrows in Chart 1 for X_1 substituent).

coordinated peroxide is induced by cysteinate as suggested by Dawson et al.[35] We believe that a similar feature may occur in the catalysis by Fe^{III}−TAMLs. Supported by the results of high pressure studies, this can account for the differences in the rate constants k_1 and k_2 (or k_3) both for H_2O_2 and ^{t}BuOOH.

***k*$_2$ versus *k*$_3$ Pathway Dilemma.** The k_2 and k_3 pathways are kinetically indistinguishable. We have previously argued that the k_2 pathway is more realistic than k_3 in view of the exceedingly large rate constants k_3 observed for H_2O_2 (ca. 10^6 M^{-1} s^{-1}).[9] The Hammett plots in Figure 10 for the rate constants k_2 and k_3 for activation of ^{t}BuOOH also support this hypothesis. The value of ρ is small and positive for k_3 ($+0.7$), but ρ is very small and negative for k_2 (-0.08).[61] Neither slope is dramatic enough to support strong interpretations, but the difference between the two is interesting. One possible interpretation is that the iron center in the k_2 pathway is weakly nucleophilic, whereas it is moderately electrophilic in the k_3 pathway. Mechanistic conclusions from the high pressure studies do not support an electrophilic nature for iron. The O−O bond cleavage is promoted by the presence of an OH^- ligand suggesting that the cleavage process requires a flow of electron density from iron(III) and therefore a nucleophilic character for iron should be anticipated. Though the absolute value of ρ (-0.08) for k_2 is extremely low, it is more negative than that for k_3. The overall process entails many steps and there should be a contribution from the pre-equilibrium binding of ^{t}BuOOH to Fe^{III} (Scheme 4) to the observed ρ values for k_2 and k_3, which should be slightly positive.[32] This could contribute to making ρ for k_2 less negative.

The activation parameters calculated for the k_2 and k_3 pathways (Table 2) are noteworthy. The enthalpy of activation is noticeably larger for the k_3 pathway, perhaps because two negatively charged species, namely, $[FeL(OH_2)_2]^-$ and ROO^-, have to meet and bind with the resulting repulsive terms adding to the activation enthalpy compared to the k_2 pathway. The activation entropy $\Delta S^{\ddagger}$ is significantly more positive for the k_3

(59) Sarauli, D.; Meier, R.; Liu, G.-F.; Ivanovic-Burmazovic, I.; van Eldik, R. *Inorg. Chem.* **2005**, *44*, 7624–7633.

(60) Basolo, F.; Pearson, A. G. *Mechanism of Inorganic Reactions. A Study of Metal Complexes in Solution*, 2nd ed.; Wiley: New York, 1967.

(61) Note that we have previously reported that the coefficient ρ of the Hammett equation equals $+0.3$ (see ref 9). This was obtained by using the effective values of k_1 measured at pH 9, i.e., without separating the rate constants k_2 and k_3. Curiously, this value is exactly the mean value of those two reported in this work ($0.5(0.7 + -0.08) \sim 0.3$).

pathway again favoring the k_2 pathway. Thus, the data to date suggest that the k_2 pathway likely dominates over the kinetically indistinguishable k_3 pathway.

Concluding Remarks. This study adds further details that support our previous mechanistic conclusions on the interactions of Fe^{III}−TAML activators with hydrogen peroxide and *tert*-butyl hydroperoxide, which in the absence of appropriate electron donors result in the generation of iron(IV) species. The iron(III)-aqua compound in pH 11 aqueous solution exhibits a peak in the differential pulse voltammogram around 0.87 V versus NHE that we ascribe to a proton-coupled electron transfer reduction of the iron(IV)-oxo complex. High-pressure kinetic studies and a Hammett analysis point to the conclusion that the k_2 pathway, involving the interaction of ROOH with $[FeL(OH_2)OH]^{2-}$, dominates over the kinetically indistinguishable k_3 counterpart, involving the interaction of $[FeL(OH_2)_2]^-$ with ROO^-. This k_2 pathway mechanistically resembles cytochrome P450 enzymes in terms of the O−O bond cleavage of coordinated peroxide.

Acknowledgment. Operating support is acknowledged from the Heinz Endowments (T.J.C.), the Institute for Green Science (T.J.C.), and the Environmental Protection Agency (Grant RD 83 to T.J.C.). A.D.R thanks the Alexander von Humboldt Foundation for the fellowship. The U.S. team acknowledges the National Science Foundation (CHE-0342742) for purchasing the stopped-flow instrument of the Department of Chemistry at Carnegie Mellon University and thanks Dr. F. Tiago de Oliveria for assistance in using the Mathematica 5 software. The German team gratefully acknowledges financial support from the Deutsche Forschungsgemeinschaft within SFB 583 on Redox-active Metal Complexes.

Supporting Information Available: Details of determination of equilibrium constant K_1. Figure S1 with the Job plot for the titration of **1a** by H_2O_2. Figures S2 and S3 showing linear dependencies of k_{obs} on concentrations of ^{t}BuOOH and H_2O_2, respectively. This material is available free of charge via the Internet at http://pubs.acs.org.